Kiegan Rice,[1,2] *M.Sc.; Ulrike Genschel*,[1,2] *Ph.D.; and Heike Hofmann*,[1,2] *Ph.D.*

A Robust Approach to Automatically Locating Grooves in 3D Bullet Land Scans*

ABSTRACT: Land engraved areas (LEAs) provide evidence to address the same source–different source problem in forensic firearms examination. Collecting 3D images of bullet LEAs requires capturing portions of the neighboring groove engraved areas (GEAs). Analyzing LEA and GEA data separately is imperative to accuracy in automated comparison methods such as the one developed by Hare et al. (Ann Appl Stat 2017;11, 2332). Existing standard statistical modeling techniques often fail to adequately separate LEA and GEA data due to the atypical structure of 3D bullet data. We developed a method for automated removal of GEA data based on robust locally weighted regression (LOESS). This automated method was tested on high-resolution 3D scans of LEAs from two bullet test sets with a total of 622 LEA scans. Our robust LOESS method outperforms a previously proposed "rollapply" method. We conclude that our method is a major improvement upon rollapply, but that further validation needs to be conducted before the method can be applied in a fully automated fashion.

KEYWORDS: land engraved areas (LEAs), groove engraved areas (GEAs), 3D scans, bullet identification, automatic matching

Forensic firearms examiners analyze bullets through a process of visual comparison to determine whether two bullets originate from the same source. Two bullets in question are placed under a comparison microscope, and firearms examiners evaluate similarities and differences between striated tool marks produced on fired bullets from rifled barrels. The assessment of these patterns follows the AFTE Theory of Identification (1) guidelines resulting in a decision about whether both bullets were fired through the same gun barrel. In forensic science, this problem is known as the *same source–different source problem* (see Ref. [2]) and it focuses on establishing quantitative evidence whether two bullets were fired through the same gun barrel.

Recent advances in technology, particularly wider access to high resolution 3D microscopy tools, have led to an increase in research on image analysis algorithms for automated, quantitative analyses of bullet evidence. The introduction of such scanning technology to the field of forensic science allows for capture of high-resolution 3D images of bullet land engraved areas (LEAs), depicted in Fig. 1 (see Refs. [3–5]). The resulting 3D images have since been used in the development of several novel methods for automated comparison of land engraved areas (e.g., Refs. [6–9]).

[1]Department of Statistics, Iowa State University, 2438 Osborn Dr., Ames, IA 50011-1090.

[2]Center for Statistics and Applications in Forensic Evidence (CSAFE),195 Durham Center, 613 Morrill Road, Ames, IA 50011.

Corresponding author: Kiegan Rice, M.Sc. E-mail: ricek@iastate.edu

*This work was partially funded by the Center for Statistics and Applications in Forensic Evidence (CSAFE) through Cooperative Agreement No. 70NANB15H176 between NIST and Iowa State University, which includes activities carried out at Carnegie Mellon University, University of California Irvine, and University of Virginia.

Received 12 June 2019; and in revised form 26 Aug. 2019, 15 Nov. 2019; accepted 4 Dec. 2019.

In this paper, we will focus only on barrels with traditional sharp-edged lands and grooves (i.e., no polygonal rifling). Sections of the bullet that make contact with high points inside the barrel are called land engraved areas (LEAs) and alternate with low points called groove engraved areas (GEAs). Micro imperfections in the barrel introduce striated tool marks on the bullet during the firing process. The resulting striation marks provide evidence to address the same source–different source problem. A guiding principle in forensic firearms analysis is that two bullets fired through the same barrel will bear more similar striation marks on their LEAs than two bullets fired from different barrels. Hare et al. (6) proposes a matching algorithm based on 3D imaging data of LEAs. Horizontal slices of the 3D images, called crosscuts, provide a detailed representation of striae engraved on the surface at a horizontal cross-section of each LEA. A current limitation of this algorithm is that it cannot deal with a mix of striae from both LEA and GEAs. For the human visual system, separating the two areas is straightforward. However, the same cannot be said for automated computer toolmark comparison techniques.

A correct identification of LEAs is vital to achieve high accuracy and precision in the subsequent downstream analysis and our goal is to present and discuss different automated methods for identifying so-called *shoulder locations*, the locations at which the land engraved areas end and the groove engraved areas begin.

One currently available method to identify these shoulder locations is the "rollapply" method proposed by (6). This method is publicly available through the "bulletxtrctr" package for the open source statistical computing language "R". The authors propose first applying a rolling average to each profile to smooth out bumps in data, followed by identifying the local minima closest to the edges of each smoothed profile.

The structure of the paper is as follows: a description of the data storage format and data set, an explanation of methodology

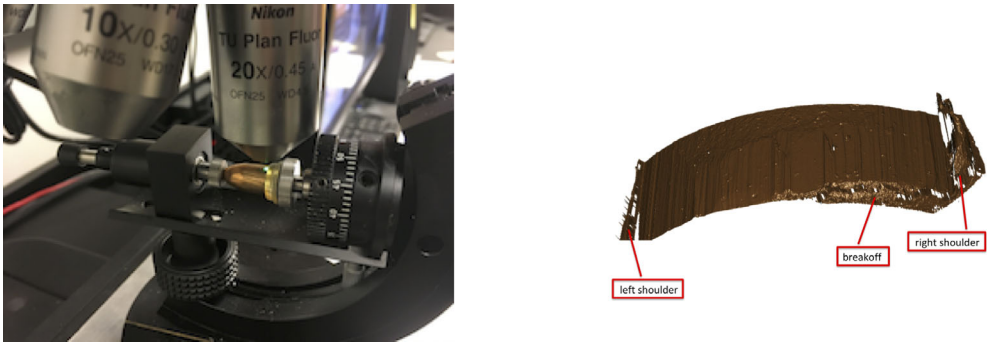

FIG. 1—*(Left) Close-up view of a bullet staged in a confocal light microscope. The green light marks the focal view of the capture area. (Right) Computer-rendered image of the scanned land engraved area with prominent striation marks. Breakoff is seen visually on the bottom right hand side on the scan.*

to predict shoulder locations, and finally an illustration of improved prediction accuracy results.

Data Source

All currently published automated methods rely on high-resolution 3D scans of bullet land engraved areas. Our approach to the collection of 3D images of bullet LEAs requires that bullets are staged such that striae appear vertically in the scan. Scanning across the LEA must begin and end in the neighboring groove engraved areas as shown in Fig. 2. Parts of the breakoff are captured as a visual reference for orientation (see Fig. 1). Scans are exported from the microscope as x3p files, conforming to the ISO5436-2 standard (10). Each scan is recorded as a matrix of prespecified (x, y) locations with a measured relative height value z for each (x, y) location on the LEA.

The algorithm proposed by Hare et al. (6) uses so-called crosscuts, height measurements along x for a fixed y. Removal of the overall curve of the bullet—the global structure captured in the 3D scanning process—transforms these crosscuts into to what Hare et al. (6) refer to as *signatures* (see Fig. 3). The assessment of similarity between two LEAs is then based on a set of extracted features such as cross-correlation function, number of consecutively matching striae (see Ref. [11]) and maximum number of consecutively non-matching striae. Successful extraction of this set of features depends on how well we can remove the global bullet structure to translate from a crosscut to the corresponding signature.

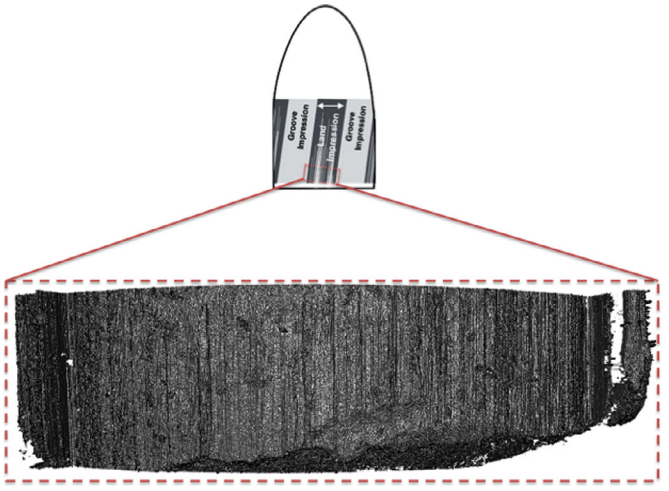

FIG. 2—*Visualization of 3D data collected through high-resolution scanning of a land engraved area. Striations on the surface of the object can be seen by viewing this data from "above," as presented here.*

In the following, we are introducing and comparing two methods for identifying shoulder locations. In order to assess the performance of these methods, we are applying both methods on 3D scans of LEAs from Hamby set 44 (12) and the Houston test set. Each Hamby set consists of 35 Winchester 9-mm copper bullets fired from 10 consecutively rifled Ruger P-85 9-mm Luger barrels. The Houston test set consists of 69 American Eagle 124 grain 9-mm copper bullets fired from Ruger LCP barrels.

Each fired bullet in Hamby set 44 and Houston test set has 6 LEAs; every LEA was scanned for each of the 104 bullets, producing data for 624 individual lands. Two lands—Barrel 9, Bullet 2, Land 3 and Questioned Bullet L, Land 5—were removed from consideration because they were deemed unsuitable for comparison. These two LEAs contained significant abrasians created by contact with the bottom of a water recovery tank after exiting the barrel. These abrasians are thus marks present on the LEAs that are not due to contact with the barrel itself.

All 3D scans of Hamby Set 44 and Houston test set were captured at Iowa State University's Roy J. Carver High Resolution Microscopy Facility with a Sensofar Confocal light microscope at 20 times magnification resulting in a resolution of 0.645 microns per pixel (1 micron = 1 μm = 0.001 mm). Physically, each land is approximately 3 mm in width; as such, data structures for a single LEA can contain more than 3 million individual data points. Data used to assess performance of the two methods consist of 2D crosscuts gathered from the 3D scans, as shown in Fig. 4.

Methodology

The structure in the 2D crosscuts is dominated by the curvature of the physical object (the bullet). To assess the similarity of features from two land engraved areas, this curvature has to be removed.

Nonparametric methods suggested in the literature, such as a LOESS fit (6) or a Gaussian filter (8) are effective for removing the curvature to extract a signature. However, they are prone to boundary effects, which cause mischaracterizations of data patterns near the boundaries of the data domain. In the case of crosscuts, the boundaries are often dominated by values originating from the GEA structure. This structure exaggerates existing

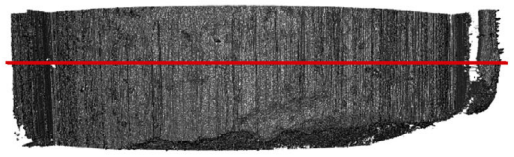

Step 1: 3D scan with identified horizontal crosscut

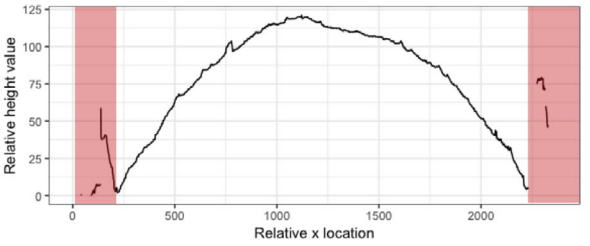

Step 2: Horizontal crosscut with identified GEA data

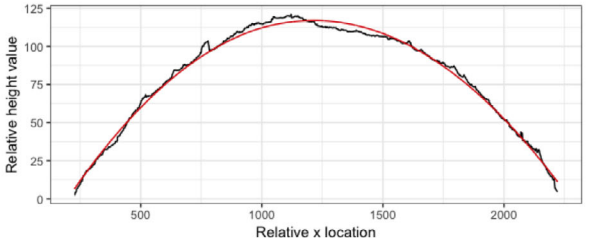

Step 3: Non-parametric curvature estimation

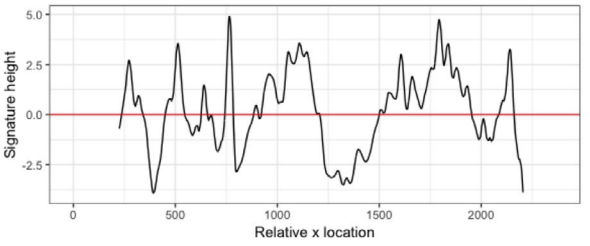

Step 4: Extracted 2D LEA signature

FIG. 3—*The process of extracting a signature from a 3D LEA scan described by Ref. (6). GEA removal between steps 2 and 3 is critical to ensure precise signature extraction.*

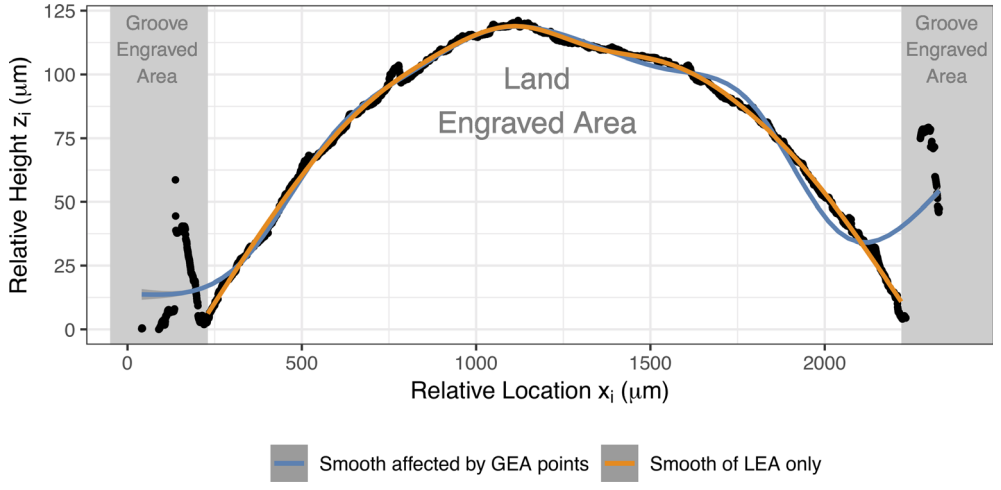

FIG. 4—*The black points show measured heights for a single crosscut of a 3D LEA scan. The main data structure, located in the center, is comprised of the land engraved area. The groove engraved areas are found on the left and right sides of the crosscut. The lines show fits of two non-parametric LOESS smooths, with and without GEA data. When GEA data are included, the smooth fails to estimate the main LEA structure near the boundaries. The LEA pictured here is Hamby 44, Barrel 10, Bullet 2, Land 2.*

boundary effects because GEAs introduce a secondary structure different from the main curvature of the LEA, as shown in Fig. 4 and Fig. 5. Figure 4 shows how much a nonparametric LOESS fit is affected by including GEA data. Figure 5 illustrates the effect the inclusion of the same has on extracted signatures. If included, GEA data result in strong boundary effects in the signatures. Statistically, GEA data introduce outliers into the LEA data. In the next sections, we introduce two methods for fitting the LEA structure. Both methods aim to describe the relationship between horizontal position and relative height on a crosscut. While the two approaches differ in methodology, they are both rooted in the ability to mitigate potential influence caused by outlying data.

In the following, we will describe the horizontal position on a crosscut of a scan as x_i and measured relative height as z_i, where $i = 1, \ldots, n$, the number of data points along a crosscut.

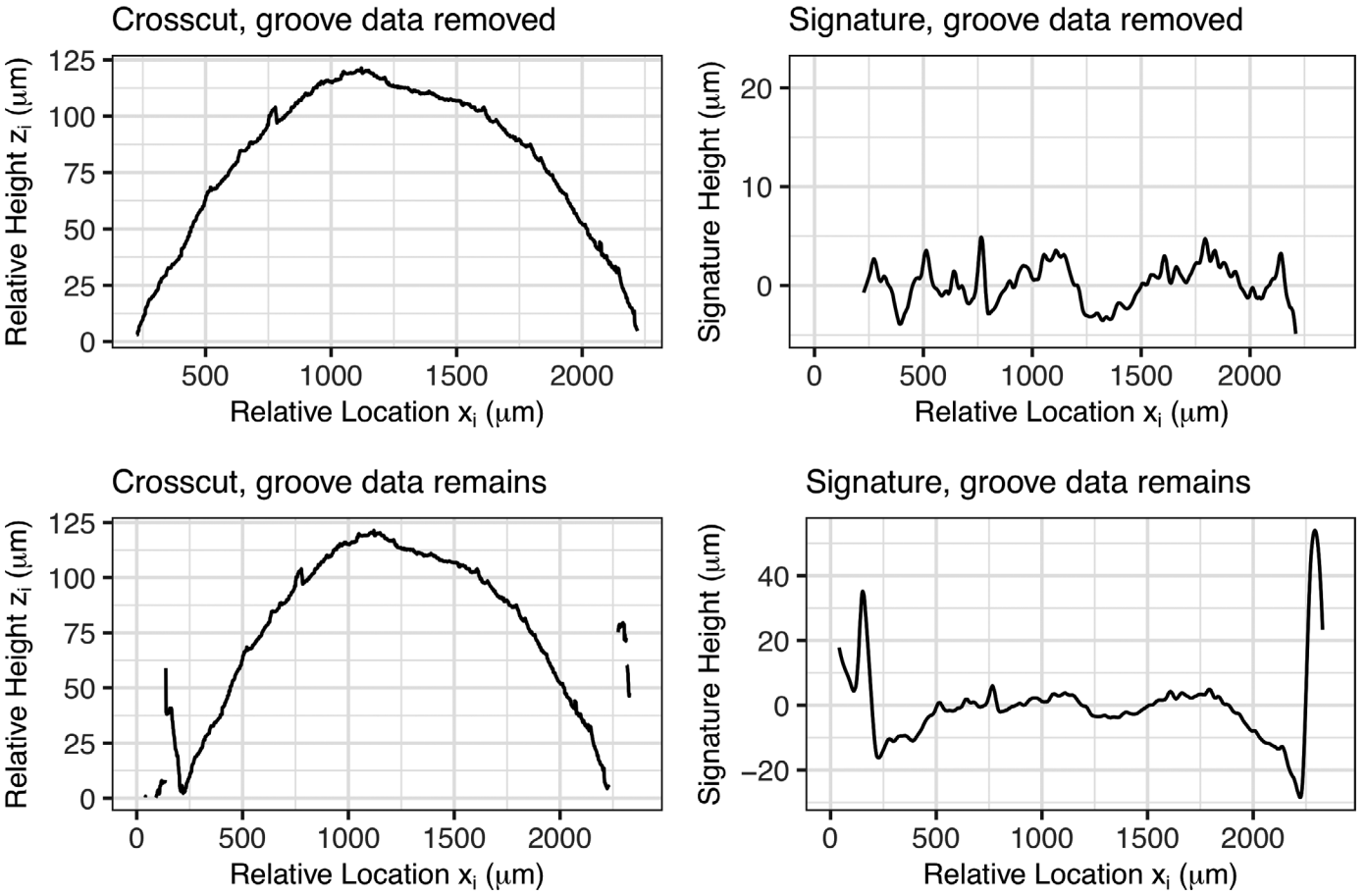

FIG. 5—*An example of the impact failure to remove GEA data can have on an extracted signature. Even though there are only very few points in the GEA structure, the extracted signatures are dominated by boundary effects. The LEA pictured here is Hamby 44, Barrel 10, Bullet 2, Land 2.*

Robust Linear Models

A natural candidate for a curved structure is a quadratic linear model of the form

$$z_i = \beta_0 + \beta_1 x_i + \beta_2 x_i^2 + \varepsilon_i,$$

where all error terms ε_i are considered independent and normally distributed with mean 0 and variance σ^2. Parameter values of β_0, β_1, β_2 are estimated by finding the values which minimize

$$\underset{\boldsymbol{\beta}}{\operatorname{argmin}} \sum_{i=1}^{n} (z_i - (\beta_0 + \beta_1 x_i + \beta_2 x_i^2))^2$$

the vertical squared distance between each measured height value and the fitted curve. Fig. 6 shows that the presence of outliers near the boundaries pulls the resulting curve upwards towards groove engraved area data.

Alternatively, the curve can be fit by minimizing the absolute deviations in place of squared deviations:

$$\underset{\boldsymbol{\beta}}{\operatorname{argmin}} \sum_{i=1}^{n} |z_i - (\beta_0 + \beta_1 x_i + \beta_2 x_i^2)|;$$

This method of minimization is less influenced by large outliers present in the GEA data and the resulting model is known as a robust linear model.

Estimation based on taking squared deviations seeks to balance the fit between the LEA structure and the GEA structure, resulting in a fit which compromises between both structures without adequately fitting either. The use of absolute deviations reduces the degree of compromise in favor of fitting the majority structure, here LEA. Figure 6*a,c* show the fitted curves from each model framework. Figure 6*b,d* display the differences between predicted height and observed height at each location x_i, known as the observed model residuals e_i. We will utilize the observed residuals to separate the two structures. The robust model in Fig. 6 fits the LEA structure more closely and better captures the curvature, allowing for a more accurate separation between GEA and LEA structures.

Because the robust approach results in residual values scattered near zero in the land engraved area and larger, mostly positive residuals in the groove engraved area, we will use high residual magnitude as an indicator of GEA membership (see Fig. 6). High residual magnitude is determined using the median absolute deviation (*MAD*) of all residuals from a crosscut.

The *MAD* is a robust metric for the spread of data, similar to the standard deviation. It is preferable to the standard deviation to quantify the spread in situations with large outlying observations, such as the residuals in the groove engraved area.

Let m denote the median function. Then the *MAD* is defined as

$$MAD(e) = m(|e_i - m(\boldsymbol{e})|) \forall e_i \in \boldsymbol{e}.$$

Any residual value larger than $4 \times MAD$ is considered an outlier and likely a member of the GEA structure.

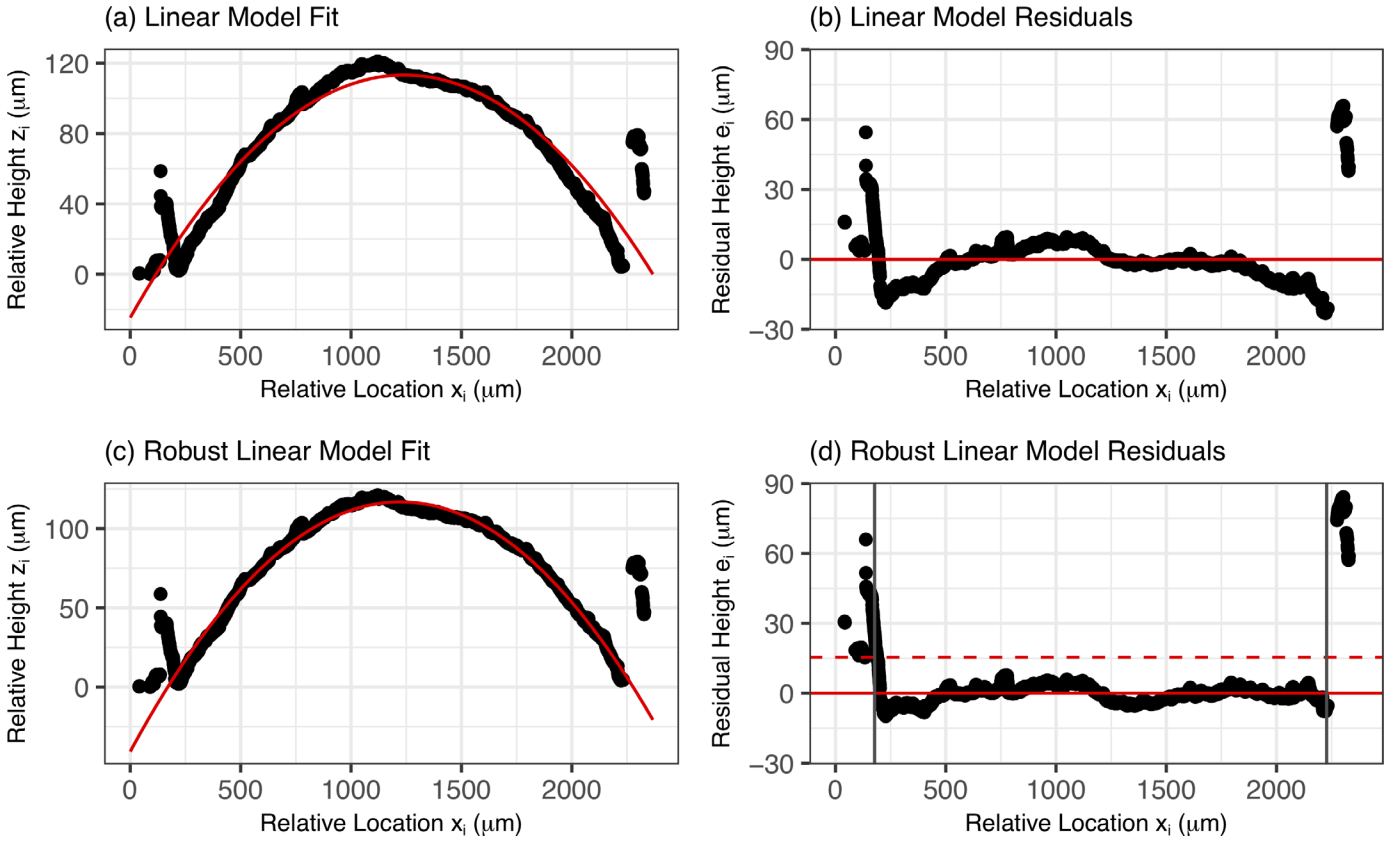

FIG. 6—*Example of a quadratic linear model fit and resulting residuals (a, b) compared to a robust quadratic linear model fit and resulting residuals (c, d) for a single crosscut. The robust model is able to more effectively capture the curved structure of the LEA without begin influenced by the GEA. The dashed line in (d) is drawn at 4 × MAD. Values above the dashed line are considered outliers. The vertical lines in (d) are drawn where the left and right shoulder locations would be identified. The LEA pictured here is Hamby 44, Barrel 10, Bullet 2, Land 2.*

Shoulder location predictions are then calculated for each crosscut in the following manner (Linear Shoulder Location Prediction):

1. Fit a robust linear model of order 2 (i.e., quadratic) to the crosscut.
2. Calculate a residual value e_i for each data point on the crosscut.
3. Calculate the residual median absolute deviation (*MAD*) for the crosscut.
4. Remove all data points on the crosscut with a residual magnitude greater than $4 \times MAD$.
5. Identify the minimum x_L and maximum x_R of the remaining x_i values. Then, x_L and x_R are the predicted left and right shoulder locations for that crosscut.

Robust LOESS

One of the drawbacks of the linear approach is its rigidity in the shape of the curve. Locally weighted regression, known as LOESS, is a more flexible approach. This is advantageous when working with bullets, as it is unrealistic to expect a circular shape to remain after the bullet has been subjected to the forces of a gun barrel.

LOESS models estimate a predicted value z_i for each height z_i corresponding to location x_i by estimating values β_0, β_1 which minimize

$$\underset{\boldsymbol{\beta}}{\operatorname{argmin}} \sum_{i=1}^{n} w_k(x_i)(z_k - (\beta_0 + \beta_1 x_k))^2, \tag{1}$$

where $w_k(x_i)$ is a weight assigned to each data point x_k based on its proximity to x_i. Weights w_k decrease as the distance to x_i increases, so that data points closest to x_i influence the prediction z_i most. A LOESS model can also be described as a non-parametric weighted average of many parametric models fit to subsets of the data.

Although this approach allows for greater flexibility, LOESS models are affected more by GEA structures than robust linear models are. Data points near and in the GEA structure are most influenced by other GEA data rather than the overall global structure. This results in a set of predictions which misrepresents much of the data near the boundaries (see Fig. 7).

Similar to the linear approach, there exists a robust approach to LOESS to adjust for these boundary effects.

The robust approach to LOESS uses an iterative re-weighting process to reduce the influence of outlying data points (see Ref. [13]). First, an initial LOESS is fit. This step is followed by a redistribution of the weights $w_k(x_i)$ based on residual values, $e_i = (z_i - \hat{z}_i)$. New weights are calculated as:

$$\left(1 - \left(\frac{e_k}{6 \times MAD}\right)^2\right)^2 \times w_k(x_i) \quad if \quad \left|\frac{e_k}{6 \times MAD}\right| < 1,$$

else, weights are set to 0. These new weights are re-applied in 1 and updated predictions are obtained. This reduces the influence

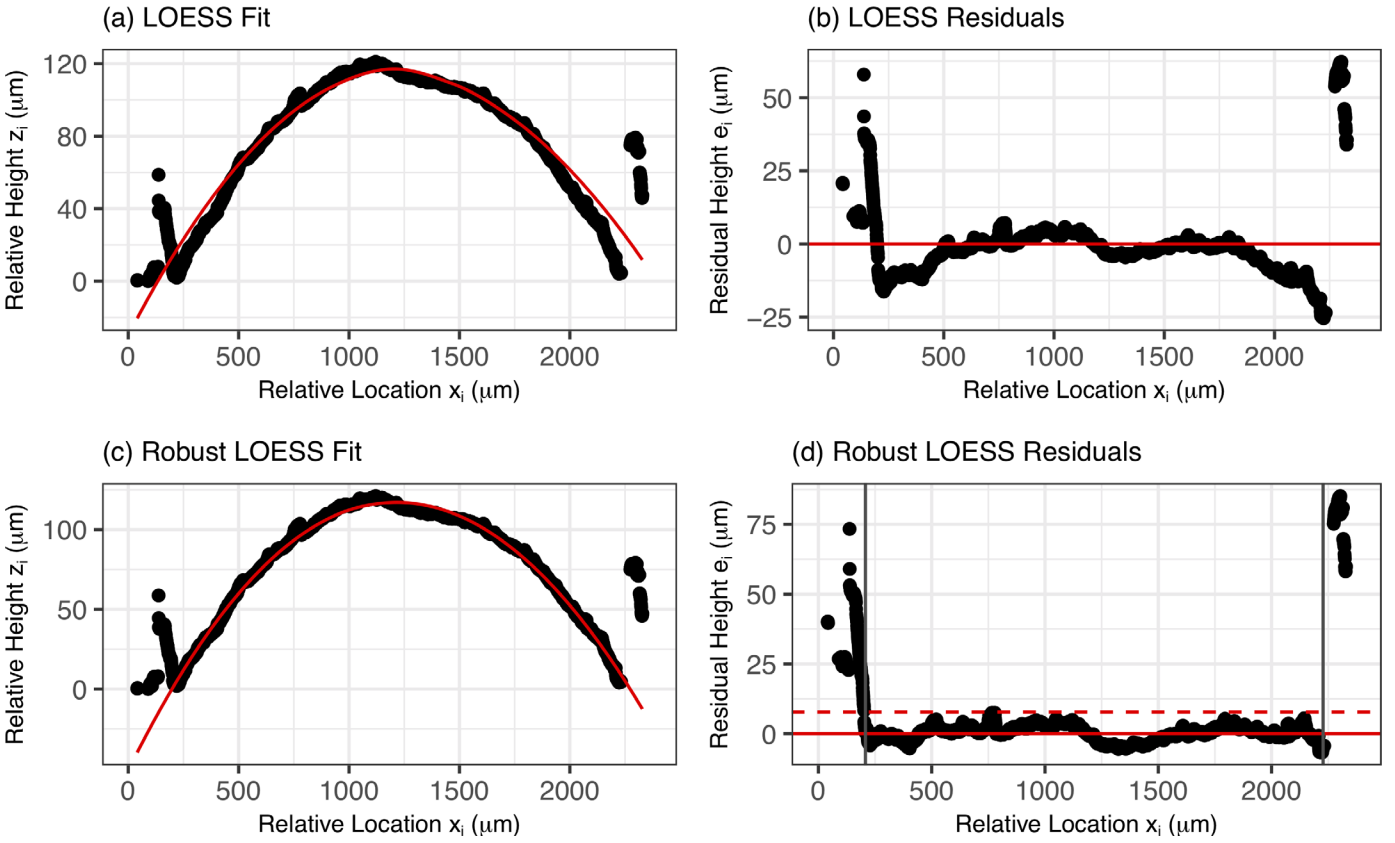

FIG. 7—*Example of a LOESS model fit and residuals (a, b) compared to a robust LOESS model fit and residuals (c, d) for a single profile. The robust model is again able to more effectively capture the curved structure of the LEA without being influenced by the GEA. The dashed line in (d) represents a cutoff of 2* × MAD. *Values above the dashed line are considered outliers. The vertical lines in (d) are drawn where the left and right shoulder locations would be identified. The LEA pictured here is Hamby 44, Barrel 10, Bullet 2, Land 2.*

of data points with large residual values e_k in subsequent iterations. In the context of LEA crosscuts, the re-weighting reduces the influence of GEA data.

A robust LOESS model which accurately fits the LEA structure should result in a similar residual structure as that expected for the robust linear model: small residuals scattered near zero for x_i locations in the land engraved area, and positive, possibly large residuals for x_i locations in the groove engraved areas. The increased flexibility of LOESS models lead to a closer fit to the curvature and thus the robust LOESS more reliably results in the aforementioned residual pattern. We can thus use a lower cutoff for separation of the residuals via magnitude. A cutoff that performs well on the Hamby set 44 and Houston test set is twice the median absolute deviation ($2 \times MAD$).

Shoulder location predictions are calculated for each crosscut in the following manner (LOESS shoulder location prediction):

1. Fit a robust LOESS model to the crosscut (14).
2. Calculate a residual value e_i for each data point on the crosscut.
3. Calculate the residual median absolute deviation (*MAD*) for the crosscut.
4. Remove all data points on the crosscut with a residual magnitude greater than $2 \times MAD$.
5. Identify the minimum x_L and maximum x_R of the remaining x_i values. Then, x_L and x_R are the predicted left and right shoulder locations for that crosscut.

Results

To quantitatively assess the predictive ability of the two alternative models, we first identified "ground truth" of shoulder locations by visual inspection for each of the 208 crosscuts in Hamby set 44 and each of the 414 crosscuts in the Houston test set.

As a performance measure, we define the error as the "area of misidentification", i.e., the area of each crosscut which is identified incorrectly by the method. This metric is calculated for the left shoulder location as

$$\hat{A}_{jL} = \sum_{e_{ij} \in X_{jL}} |e_{ij}| \times (x_{i+1} - x_i),$$

where X_{jL} is the set of points in crosscut j that fall between the predicted and actual left shoulder location, e_{ij} corresponds to the residual value at location x_i from the robust LOESS fit to crosscut j, and $(x_{i+1} - x_i)$ is the distance between two subsequent locations in the crosscut. For the scans of Hamby set 44 and Houston test set, this distance is equal to 0.645 μm for all locations.

Similarly, the area is calculated for the right shoulder location as

$$\hat{A}_{jR} = \sum_{e_{ij} \in X_{jR}} |e_{ij}| \times (x_{i+1} - x_i),$$

where X_{jR} is the set of points in crosscut j that fall between the predicted and actual right shoulder location.

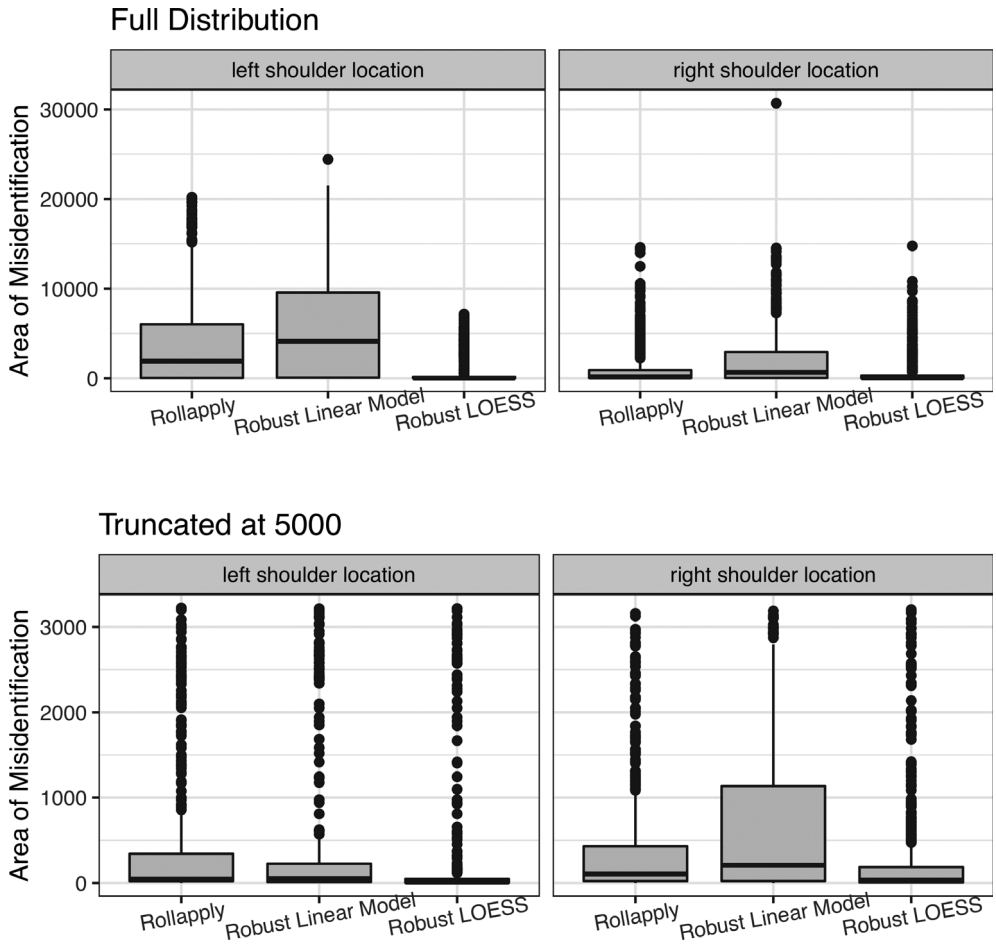

FIG. 8—*Distribution of all 622 crosscuts, presented here as a boxplot, of areas of misidentification for rollapply (data smoothing) method, robust linear model method, and robust LOESS method, separated by left and right shoulder locations. A dense distribution with few high values indicates good performance across the LEAs in the data set.*

Both the left and right areas of misidentification are thus in terms of microns^2 and represent the area of loss we incur from incorrectly identifying a shoulder location.

Quantifying the results as an area is preferable to a distance metric as it captures not only the width of the profile area that is misidentified, but also the relative heights of the data. Larger misidentified areas indicate larger portions of the GEA remain included in a profile, and thus signal an area which is more likely to have influence on an extracted signature. Smaller areas of misidentification suggest minimal loss in incurred, and these areas will have minimal effect on an extracted signature.

An area of misidentification was calculated separately for the left hand side and right hand side predictions for each of the 622 profiles in the data set, where predictions were based on the robust linear model and robust LOESS methods, as well as the rollapply method suggested in Hare et al. (6).

To assess the performance of all three methods, we consider the distribution of the areas of misidentification across all 622 lands of Hamby set 44 and the Houston test set. Figure 8 presents each distribution as a boxplot. The box encompasses the middle 50% of values, spanning the 25th to 75th percentile. The line inside each box represents the median value, and individual data points are unusually large values we call outliers. A distribution starting at or close to zero with minimal spread is ideal as this suggests many of the predicted shoulder locations are very close to the manually identified locations, and predictions are removing many of the outlying GEA points. A distribution with a wider spread or many high, outlying areas of misidentification suggests a greater degree of uncertainty and inaccuracy for a particular method. Some of the outliers are so extreme, statistics appear very close to one another or on top of each other.

Because the raw distributions are difficult to visually compare due to extreme outliers, we categorized areas of misidentification as small, medium, or large deviations and divided results between the two test sets. Scores under 100 are considered small deviations, scores between 100 and 1000 are medium, and scores above 1000 are considered large deviations (see Fig. 9). Note that this binning could be done differently. We simply want a rough categorization of different levels of deviation from the ground truth shoulder location. Cases with large deviations are the most likely to cause poor or flawed results in subsequent analyses. Note that Fig. 9*a* and Table 1, as well as Fig. 9*b* and Table 2, are based on the same numbers but provide two different presentations of the results.

It is important to note that different results are expected for the left and right shoulder locations. Within Hamby set 44 and Houston test set, almost all scans have a well-defined left groove. Left here is defined as visually left on the scan; this is the side the scan begins on, so a well-defined distinction between GEA and LEA is expected. Often, a less clear distinction is seen on the right side of the scan, with sometimes no

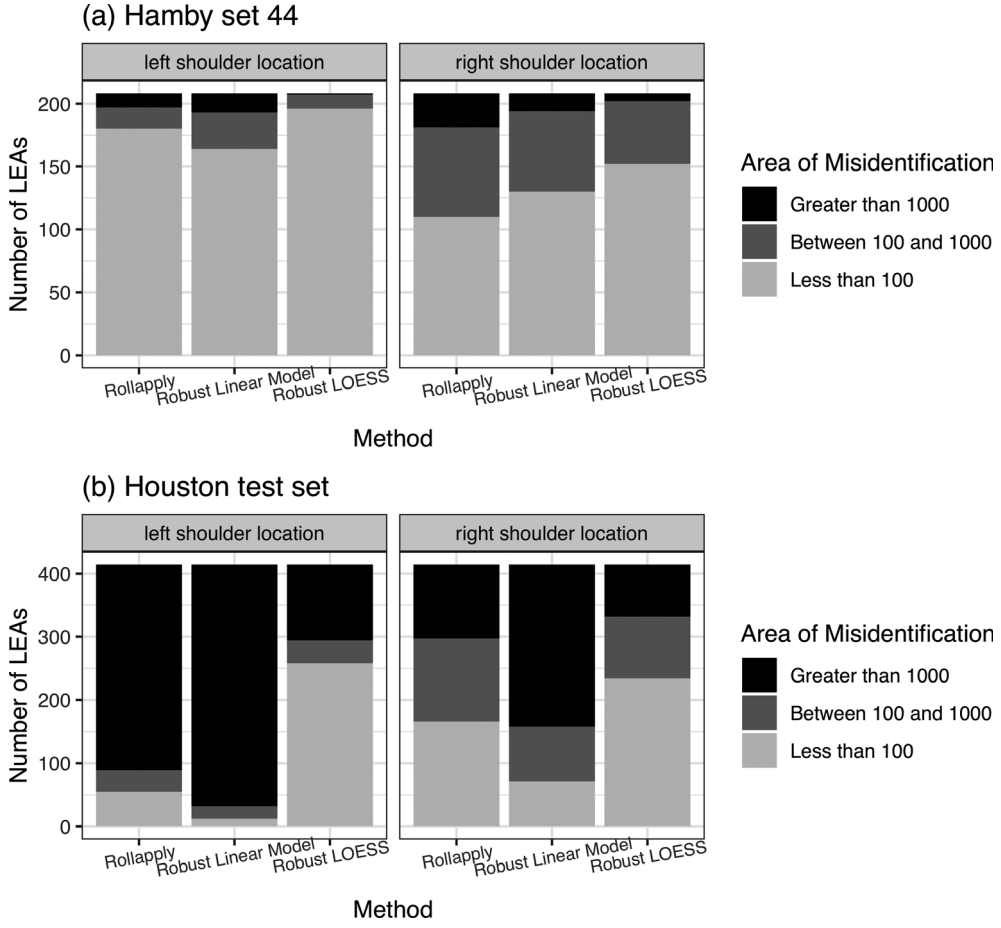

FIG. 9—*Distribution of areas of misidentification for rollapply (data smoothing) method, robust linear model method, and robust LOESS method, separated by left and right shoulder location. Areas of misidentification are placed into three categories: less than 100 microns squared (small deviations), between 100 and 1000 microns squared, and greater than 1000 microns squared (large deviations). A larger proportion of areas of misidentification under 100 microns squared indicates good performance across LEAs in the data set. Results are split between Hamby set 44 and the Houston test set.*

TABLE 1—*Table of results for areas of misidentification (in μm^2) resulting from automated shoulder location identification methods applied to Hamby set 44. Results are presented as percentage of shoulder location predictions which fall into each category: satisfactory (less than 100), borderline (between 100 and 1000), and unsatisfactory (greater than 1000).*

	Left Shoulder Location			Right Shoulder Location		
Method	(0, 100)	(100, 1000)	(1000, ∞)	(0, 100)	(100, 1000)	(1000, ∞)
Rollapply	86.54	8.17	5.29	52.88	34.13	12.98
Robust linear model	78.85	13.94	7.21	62.50	30.77	6.73
Robust LOESS	94.23	5.29	0.48	73.08	24.04	2.88

TABLE 2—*Table of results for areas of misidentification (in μm^2) resulting from automated shoulder location identification methods applied to the Houston test set. Results are presented as percentage of shoulder location predictions which fall into each category: satisfactory (less than 100), borderline (between 100 and 1000), and unsatisfactory (greater than 1000).*

	Left Shoulder Location			Right Shoulder Location		
Method	(0, 100)	(100, 1000)	(1000, ∞)	(0, 100)	(100, 1000)	(1000, ∞)
Rollapply	13.29	8.21	78.50	40.10	31.64	28.26
Robust linear model	2.90	4.82	92.27	17.15	21.01	61.84
Robust LOESS	62.32	8.70	28.99	56.52	23.67	19.81

apparent shoulder location visible. This may be due to the right shoulder corresponding to the leading edge in the twist of a bullet as it is propelled through a gun barrel. For this reason it is preferable to separate the left and right for visual inspection of results; a method may excel on one side but fall short on another.

Conclusions

The robust LOESS approach clearly outperforms both the robust linear model and the rollapply method for both the left and right shoulder locations on both Hamby set 33 and the Houston test set. While the robust linear model approach outperforms rollapply for the right shoulder location on Hamby set 44, it performs the worst for both sides of the Houston test data and the left shoulder location of Hamby set 44. This hierarchy of performance is well within expectation given the strength of robust approaches in general as well as the flexibility of LOESS applied to this data type. Robust LOESS also readily handles variation introduced in the process of translating the physical bullet into a 3D object. If there is too much variability in how

the bullet is placed relative to the plane of reference on the microscope, profiles can have tilted shapes relative to the *x*-axis, which a quadratic linear model would fail to address. In these situations, LOESS excels.

While the proposed cutoff value as a multiple of *MAD* works well for robust LOESS on Hamby set 44 and Houston test, additional validation will need to be executed on a wider variety of barrel types. Depth of striae, physical size of bullet due to caliber, and nontraditional rifling techniques may require alterations to this cutoff value. LEAs with shoulders which are not horizontally aligned due to tilt may also require slight alterations to this method. In addition, a study of the effect of implementing robust LOESS shoulder location identification on the downstream similarity assessment will need to be completed. Due to increased accuracy of predicted shoulder locations, the authors expect an increase in accuracy in bullet matching algorithms. However, this will need to be validated on a variety of data sets prior to implementation without human intervention in the automated process.

Acknowledgments

We would like to thank the efforts of the Center for Statistics and Applications in Forensic Evidence (CSAFE) and the Roy J. Carver High Resolution Microscopy laboratory in scanning the Hamby set 44 and Houston test set and providing the scans to us.

References

1. Glossary AFTE. Theory of identification as it relates to toolmarks. AFTE J 1998;30(1):86–8.
2. Ommen DM, Saunders CP. Building a unified statistical framework for the forensic identification of source problems. Law Probab Risk 2018;17 (2):179–97.
3. De Kinder J, Prevot P, Pirlot M, Nys B. Surface topology of bullet striations: an innovating technique. AFTE J 1998;30(2):294–9.
4. De Kinder J, Bonifanti M. Automated comparison of bullet striations based on 3D topography. Forensic Sci Int 1999;101:85–93.
5. Bachrach B. Development of a 3D-based automated firearms evidence comparison system. J Forensic Sci 2002;47(6):1253–64.
6. Hare E, Hofmann H, Carriquiry A. Automatic matching of bullet land impressions. Ann Appl Stat 2017;11(4):2332–56.
7. Ma L, Song J, Whitenton E, Zheng A, Vorburger T, Zhou J. NIST bullet signature measurement system for RM (Reference Material) 8240 standard bullets. J Forensic Sci 2004;49(4):649–59.
8. Chu W, Song T, Vorburger J, Yen J, Ballou S, Bacharach B. Pilot study of automated bullet signature identification based on topography measurements and correlations. J Forensic Sci 2010;55(2): 341–7.
9. Chu W, Thompson RM, Song J, Vorburger TV. Automatic identification of bullet signatures based on consecutive matching striae (CMS) criteria. Forensic Sci Int 2013;231(1–3):137–41.
10. ISO 5436–2:2012. Geometrical product specifications (GPS) – surface texture: profile method; Measure- ment standards – Part 2: software measurement standards. Geneva, CH: International Organization for Standardization, 2012.
11. Biasotti AA. A statistical study of the individual characteristics of fired bullets. J Forensic Sci 1959;4(1):34–50.
12. Hamby JE, Brundage DJ, Thorpe JW. The identification of bullets fired from 10 consecutively rifled 9mm Ruger pistol barrels: a research project Involving 507 participants from 20 countries. AFTE J 2009;41 (2):99–110.
13. Cleveland WS. Robust locally weighted regression and smoothing scatterplots. JASA 1979;74(368):829–36.
14. Loader C.locfit: local regression, likelihood and density estimation. 2013. R package version 1.5-9.1. https://CRAN.R-project.org/package=locfit (accessed December 4, 2019).